INSTITUTE OF PHYSICS PUBLISHING JOURNAL OF PHYSICS A: MATHEMATICAL AND GENERAL

J. Phys. A: Math. Gen. **36** (2003) 4221–4237 PII: S0305-4470(03)39230-3

Spurious internal fields in scattering by a cylinder

J F Nye

Department of Physics, University of Bristol, UK

Received 9 July 2002, in final form 20 January 2003
Published 26 March 2003
Online at stacks.iop.org/JPhysA/36/4221

Abstract

Numerical computations of scattering of electromagnetic waves by hollow conductors can produce spurious internal fields. This well-known effect is examined in detail, at an elementary level, for two-dimensional scattering by a circular cylinder. A plane electromagnetic wave of fixed frequency is scattered from a perfectly conducting hollow circular cylinder. The scattered wave may be regarded as produced by a current density in the cylindrical boundary, which can be readily computed from standard theory. Alternatively, the boundary may be divided into N discrete intervals and the current density may be computed by expressing an appropriate integral equation in discretized form. There is then a difference between the computed and exact current densities that is purely an artefact of the discretization. Provided the radius is not chosen to correspond to an internal resonance, the error in the current density does approach zero as N increases, but in an unusual way: if the radius is just below a resonance value, it can increase to large values before it decreases. As well as giving some error in the computed scattered field, a conspicuous consequence is a spurious internal field, which consists of a mixture of standing waves, not normal modes of the cylinder except at resonance, one from each Fourier component of the incident plane wave.

PACS numbers: 42.25.Fx, 02.30.Rz, 02.60.−x

1. Introduction

It is well known that numerical computation of the two-dimensional external scattering of a monochromatic plane electromagnetic wave by a hollow conducting object can lead to a difficulty. Burton and Miller (1971) pointed out that there is a lack of uniqueness in the solution whenever the wave number coincides with a resonant wave number for an associated interior problem. A given scattering problem may be reduced to solving an integral equation on the boundary. Using this method Kleinman and Roach (1974), Martin (1982), Luz *et al* (1997) and Chen *et al* (2001), among others, have shown how the problem of non-uniqueness may be approached and have devised ways of dealing with it; Benthien and Schenck (1997) provide a useful review. A consequence of the lack of uniqueness at wave numbers corresponding to

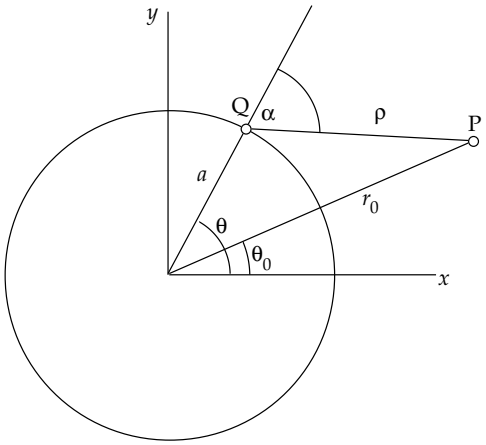

Figure 1. E-polarization. Notation.

internal resonances is the appearance in numerical solutions of internal standing waves even when theoretically none should be present. More seriously, such spurious internal waves can appear even quite far from a resonance, a problem that becomes worse as the resonances get closer together.

This paper traces in detail, at an elementary level, how these effects arise with a cylindrical boundary, using the simplest method of solution for the two integral equations corresponding to the two different polarizations. For a cylindrical boundary there are well-known exact analytical solutions, and so the origin of the spurious waves can be clearly understood.

2. Scattering by a cylinder

A plane electromagnetic wave travelling along the x axis from positive to negative is incident upon a hollow, perfectly conducting cylinder whose axis is O_z (figure 1). The two different polarizations to be considered are: (1) E-polarization, where the electric vector in the incident wave is parallel to O_z, and (2) B-polarization, where **B** in the incident wave is parallel to O_z. In both cases the solution is independent of z. In case (1) the equivalent scalar problem has a scalar wave $u = E_z$ incident, with the Dirichlet boundary condition $u = E_z = 0$ on the cylinder. In case (2) the equivalent scalar problem has a scalar wave $u = B_z$ incident, with the Neumann boundary condition $\partial u/\partial r \propto E_\theta = 0$ on the cylinder. Given the two scalar solutions the other non-zero components of the field are readily obtained by differentiation from Maxwell's equations (Born and Wolf 1999, section 11.4.1).

3. E-polarization

This is the more straightforward of the two cases. Let the incident wave have unit amplitude of electric field and wave number κ with time dependence $e^{-i\omega t}$. Write the space-dependent part as $E_z^{\text{inc}} = u^{\text{inc}} = e^{-i\kappa x}$, use polar coordinates r, θ and expand in terms of Bessel functions $J_m(\kappa r)$, thus (Morse and Feshbach 1953)

$$u^{\text{inc}} = e^{-i\kappa x} = \sum_{m=0}^{\infty} \varepsilon_m (-i)^m J_m(\kappa r) \cos m\theta \tag{1}$$

where

$$\varepsilon_m = \begin{cases} 1 & \text{if} \quad m = 0 \\ 2 & \text{if} \quad m > 0. \end{cases}$$

The scattered wave must be of the form

$$u^{\text{sc}} = \sum_{m=0}^{\infty} C_m H_m^{(1)}(\kappa r) \cos m\theta \tag{2}$$

where the $H_m^{(1)}(\kappa r)$ are Hankel functions of the first kind, corresponding to outgoing waves. Henceforward we shall omit the superscript (1). From the condition $u^{\text{total}} = u^{\text{inc}} + u^{\text{sc}} = 0$ on the boundary $r = a$, it follows that for each term

$$C_m = -\frac{\varepsilon_m(-\text{i})^m J_m(\kappa a)}{H_m(\kappa a)}.$$

Thus the total wave is

$$u^{\text{total}} = \sum_{m=0}^{\infty} \varepsilon_m(-\text{i})^m \cos m\theta \left[J_m(\kappa r) - \frac{J_m(\kappa a)}{H_m(\kappa a)} H_m(\kappa r) \right]. \tag{3}$$

This is the required well-known solution for the field outside the boundary cylinder.

We now examine an alternative approach in which the scattered field is regarded as being caused by a surface current in the cylinder flowing in the z direction with density $j_z(\theta)$. We can find j_z from the above solution by noting that it is given by the discontinuity in B_θ at the boundary. In general, from Maxwell's equations,

$$B_\theta = \frac{\text{i}}{\kappa \text{c}} \frac{\partial u^{\text{total}}}{\partial r} \qquad \text{and} \quad \mu_0 j_z = B_\theta^+ - B_\theta^- \tag{4}$$

where + and − refer to the outside and inside, respectively. If we assume that there is no field inside the cylinder, by screening, then $j_z = \mu_0^{-1} B_\theta^+ = \frac{\text{i}}{\kappa Z_0}\left(\frac{\partial u^{\text{total}}}{\partial r}\right)_{r=a}$, where we have written $\kappa c \mu_0 = \kappa Z_0$ with $Z_0 = \sqrt{\mu_0/\varepsilon_0}$. Carrying out the differentiation of (3) and setting $r = a$ we have

$$\frac{1}{\kappa}\left(\frac{\partial u}{\partial r}\right)_{r=a} = \sum_{m=0}^{\infty} \varepsilon_m(-\text{i})^m \cos m\theta \left[\frac{J_m'(\kappa a) H_m(\kappa a) - J_m(\kappa a) H_m'(\kappa a)}{H_m(\kappa a)} \right]. \tag{5}$$

Writing $H_m = J_m + \text{i}Y_m$ and using the Wronskian relation $J_m Y_m' - J_m' Y_m = (2/\pi\kappa a)$ then gives

$$j_z(\theta) = \frac{2}{\pi \kappa a Z_0} \sum_{m=0}^{\infty} \varepsilon_m(-\text{i})^m \cos m\theta \frac{1}{H_m(\kappa a)}. \tag{6}$$

In the absence of any free oscillations within the cylinder (see below) the current density found in this way is exact, and will be designated as $j_z^{\text{true}}(\theta)$. By construction, it produces the scattered wave E_z^{sc}outside the circle and $-E_z^{\text{inc}}$ inside, to give $E_z^{\text{total}} = 0$. It is simple to compute $j_z^{\text{true}}(\theta)$ to any desired accuracy from equation (6). The series must be terminated only when two successive terms become less than a set value ε (in units of Z_0^{-1}). Thus, for example, if $\varepsilon = 10^{-6}$, $\kappa a = 1$ requires 10 terms, while $\kappa a = 20$ requires 40 terms. Figure 2 shows the amplitude and phase of $j_z^{\text{true}}(\theta)$ for various κa. For small a the current density approaches infinity (with a phase of $\frac{1}{2}\pi$), but the current itself, namely $2\pi a j_z$, approaches zero. For large κa the current density at the back of the cylinder falls to zero, unsurprisingly.

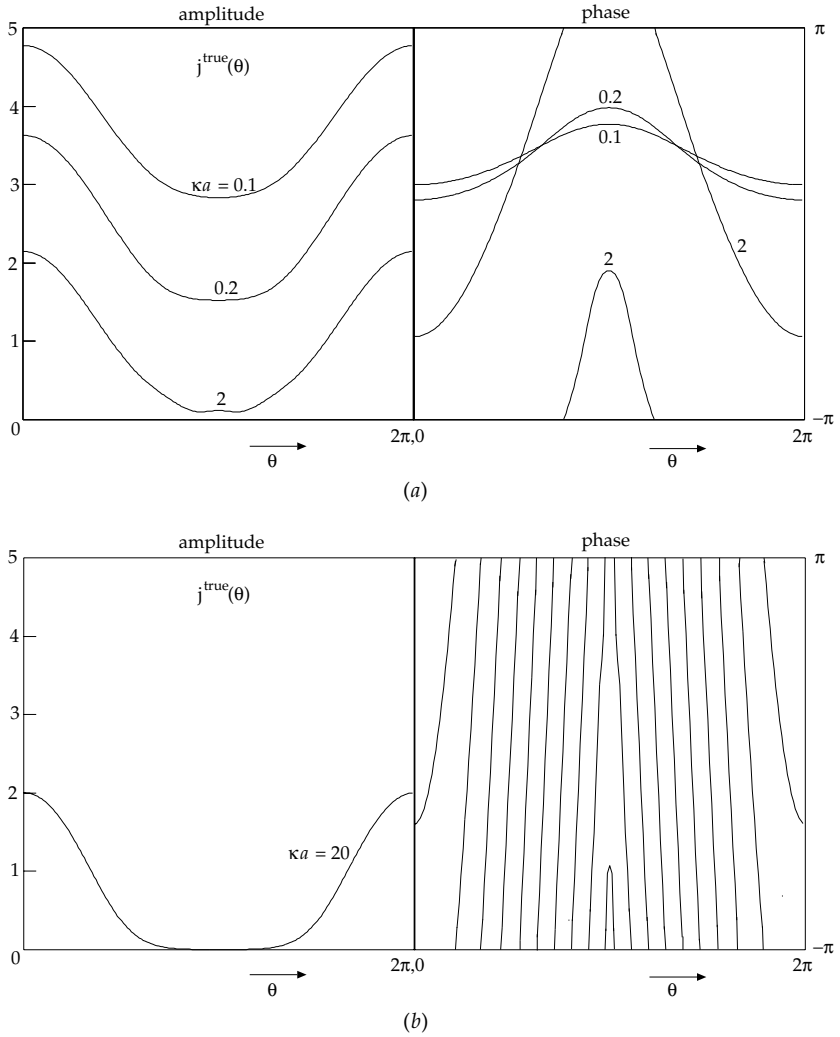

Figure 2. E-polarization. $j_z^{\text{true}}(\theta)$ for various κa. The units of $j_z^{\text{true}}(\theta)$ are Z_0^{-1}.

3.1. Solution in terms of the current sources

This alternative computational approach follows the method used in (Nye 2002) to find the exact diffraction field for several parallel slits in a conducting screen. The magnetic potential $\mathbf{A} = (0, 0, A_z)$ at any fixed point $P = (r_0, \theta_0)$ is given as an integral over the boundary circle of the current density $j_z(\theta)$ at the variable point $Q = (a, \theta)$ by

$$A_z = \frac{\mathrm{i}\mu_0 a}{4} \int_0^{2\pi} \mathrm{d}\theta \; j_z(\theta) H_0(\kappa\rho)$$

where ρ is the distance PQ (figure 2). The electrostatic potential is zero, because $j_z(\theta)$ is uniform with z and there is no accumulation of charge. The scattered electric field is then given simply by $E_z^{\text{sc}} = \mathrm{i}\omega A_z$. Hence

$$E_z^{\text{sc}} = -\frac{Z_0 \kappa a}{4} \int_0^{2\pi} \mathrm{d}\theta \; j_z(\theta) H_0(\kappa\rho). \tag{7}$$

The boundary condition is that, at points on the circle $r_0 = a$, this scattered field just cancels the incident field, to give zero total field. Thus

$$\frac{Z_0 \kappa a}{4} \int_0^{2\pi} \mathrm{d}\theta \; j_z(\theta) H_0(\kappa\rho) = \mathrm{e}^{-\mathrm{i}\kappa a \cos\theta_0}. \tag{8}$$

Since P is now on the circle, $\rho = \left|2a \sin \frac{1}{2}(\theta - \theta_0)\right|$. In principle, this integral equation may be solved to find $j_z(\theta)$. Up to this point all is straightforward and well known.

These results in conjunction with equations (6) and (7) imply the following mathematical identities when κa satisfies the resonance condition $J_m(\kappa a) = 0$. For all positions of $P = (r_0, \theta_0)$ outside or on the circle

$$\int_0^{2\pi} \mathrm{d}\theta \cos m\theta \, H_0(\kappa\rho) = 0 \tag{9}$$

where $\rho = PQ$. For all positions of P inside the circle,

$$\int_0^{2\pi} \mathrm{d}\theta \cos m\theta \, H_0(\kappa\rho) = 2\pi \, H_m(\kappa a) J_m(\kappa r_0) \cos m\theta_0. \tag{10}$$

The main point of this paper is that, for certain ranges of κa near internal resonances, the solution of (8) computed numerically, which we shall call $j_z^{\mathrm{com}}(\theta)$, does not agree satisfactorily with the correct solution $j_z^{\mathrm{true}}(\theta)$ given by equation (6). The effect of the disagreement is most conspicuous inside the boundary, for when $j_z^{\mathrm{com}}(\theta)$ is substituted in equation (7) it gives a scattered field inside that does not properly cancel the incident field, thereby producing a spurious non-zero internal field. It also produces an unexpectedly high error in the field outside.

We have so far ruled out free oscillations within the cylinder by insisting that the interior field is zero. The term on the right-hand side of equation (8) may be thought of as a forcing term and may be expanded as a Fourier series by setting $r = a$ in equation (1). Consider the situation when there is only a single forcing term, the mth term. If we also suppose that κa is such that it is the nth root of $J_m(\kappa a) = 0$, that is, an (m, n)th order resonance, equation (1) shows that the forcing term becomes zero. A possible solution is now that there is zero current and the field is simply the standing wave $u = \varepsilon_m(-\mathrm{i})^m J_m(\kappa r) \cos m\theta$, both inside and outside the circle. There is no discontinuity in gradient across the circle, and so no current. The boundary condition is satisfied, because $J_m(\kappa a) = 0$ and the boundary is a nodal surface. With no current there is no scattered wave; it is as if the boundary were transparent. This is a very simple example of the interior/exterior duality studied by Smilansky and his colleagues on which there is an extensive literature (e.g., Berry 1994, Dietz *et al* 1995). Note that the result only applies when $J_m(\kappa a) = 0$ exactly.

When $J_m(\kappa a) = 0$ we can add to the zero current solution, with its total interior field $u = \varepsilon_m(-\mathrm{i})^m J_m(\kappa r) \cos m\theta$, an additional interior scattered field $u = A J_m(\kappa r) \cos m\theta$, where A is an arbitrary complex constant. This will be associated with a current proportional to $A \cos m\theta$, and we know from equation (9) that this produces a zero scattered wave outside the circle, as well as the scattered field $A J_m(\kappa r) \cos m\theta$ inside the circle. This internal resonance has infinite Q and so the result applies only when κa has exactly the required value.

3.2. The discretized integral equation

The integral equation (8) was solved for $j_z(\theta)$ numerically, by putting it into discrete form. Expressing the integral as a summation over N points equally spaced by $\Delta\theta$ gives N linear equations of the form

$$L_{ik} j_k = R_i \qquad i, k = 1, \ldots, N \tag{11}$$

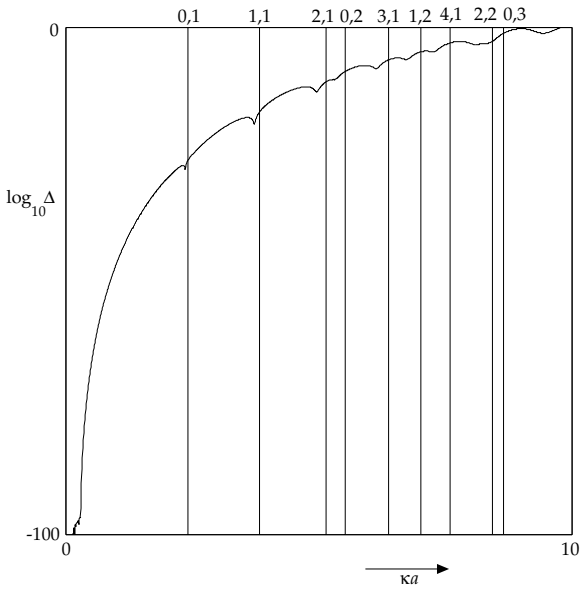

Figure 3. E-polarization. $\det(L_{ik})$ is plotted logarithmically against κa, to show the resonances (m, n). $(N = 40)$.

where each row of the matrix L_{ik} corresponds to a value of θ_0 and each column to a value of θ. The terms on the leading diagonal have $\rho = 0$, and therefore a logarithmic singularity in the imaginary part of $H_0^{(1)}(\kappa\rho)$. The infinite value is replaced by the ordinate $(2/\pi)[\ln(\Delta\theta\gamma_s/4) - 1]$, where $\ln\gamma_s = \gamma = 0.577\ldots$, to give the correct value for the summation over the two neighbouring intervals. Equations (11) were then solved for the j_k by matrix inversion, thus, in matrix form

$$j = L^{-1}R. \tag{12}$$

The solution of this equation depends on the size of the matrix and we shall denote it by $j_z^{\mathrm{com}}(N, \theta)$. The relation between $j_z^{\mathrm{com}}(N, \theta)$ and the solution $j_z^{\mathrm{true}}(\theta)$ of the true integral equation is our focus of interest, because the behaviour for special ranges of κa makes it far from straightforward. As has been remarked $j_z^{\mathrm{com}}(N, \theta)$ for finite N, does not in general agree with $j_z^{\mathrm{true}}(\theta)$. In particular, we shall not assume that the limit of $j_z^{\mathrm{com}}(N, \theta)$ as $N \to \infty$ will be $j_z^{\mathrm{true}}(\theta)$, as found from equation (6). The discrepancies are most marked near resonances.

If the right-hand side of (11) is replaced by zero the resulting set of equations would have a non-zero solution if $\det(L_{ik}) = 0$. In fact this never happens for a matrix of finite size. Plotting the determinant against κa for a given size of matrix $N \times N$ gives a curve (figure 3) showing dips which are all slightly to the left of the resonance values of κa. This is an effect of the finite size of the matrix: as N is increased the dips become deeper and their positions approach the resonance values. Owing to the banded nature of the matrix the sum of each row (and column) is the same. If this sum were zero the determinant would also be zero, but for finite N that condition is only fulfilled approximately (the equations are ill-conditioned), near the resonance values of κa.

Let us see what $j_z^{\mathrm{com}}(N, \theta)$ will be when κa is set at (in practice very close to) a resonance value. R_i on the right-hand side of equation (11) derives from $\mathrm{e}^{-\mathrm{i}\kappa a\cos\theta_0}$ on the right-hand side of equation (8), and from equation (1) may be expanded as the Fourier cosine series $\sum_{m=0}^{\infty}\varepsilon_m(-\mathrm{i})^m J_m(\kappa a)\cos m\theta$. Consider the situation where there is only a single forcing

term, the mth term, on the right-hand side. Then $j_z^{\rm com}(N,\theta)$ also will contain only a single term in $\cos m\theta$. Now choose κa to be one of the zeros of $J_m(\kappa a)=0$, so that the mth Fourier component of the right-hand side is in fact zero. The mth Fourier component of $j_z^{\rm com}(N,\theta)$ is given by $j=L^{-1}R$ with R zero. L^{-1} is not infinite for any finite N ($\det(L_{ik})\neq 0$), and hence the mth Fourier component of $j_z^{\rm com}(N,\theta)$ is exactly zero. But if $j_z^{\rm com}(N,\theta)$ is zero it can generate no scattered field; the circle is transparent. This is just the zero current solution we noted in section 3.1, in which the field inside the circle is simply the mth Fourier component of $E_z^{\rm inc}$ namely $\varepsilon_m(-{\rm i})^m J_m(\kappa r)\cos m\theta$. This result is independent of the size N of the matrix, but of course it only applies at the values of θ that are sampled. It is crucial that the result depends on L^{-1} not being infinite, whereas in the ideal case it would be infinite, and would therefore allow a finite but indeterminate j_z (with an arbitrary complex factor A).

In summary, if κa is chosen to be close to one of the zeros of $J_m(\kappa a)=0$, and if we consider only the mth term in the incident wave, the matrix equation (12) will generate a current density $j_z^{\rm com}(N,\theta)=0$, which will lead numerically to a total internal field $\varepsilon_m(-{\rm i})^m J_m(\kappa r)\cos m\theta$, which is the mth Fourier component of the incident field (a standing wave, with a uniform phase of 0, $\pm\frac{1}{2}\pi$ or $\pm\pi$ apart from jumps of π where $J_m(\kappa r)$ or $\cos m\theta$ changes sign). Since this will happen however large N may be, whereas the true internal field is zero, it shows that the matrix method is bound to fail when κa is very close to resonance.

3.3. The approach to the limit

Now consider the values found for $j_z^{\rm com}$ when κa is not necessarily set at a resonance value. Figure 4 is constructed by taking for R_i in equation (12) simply its first Fourier component (using $m=1$ purely for illustration) and computing $j^{\rm com}$ and $j^{\rm true}$ (the suffix z is to be understood). (Since they are both proportional to $\cos\theta$ it is convenient to compute them only at $\theta=0$.) In figure 4(a) $j^{\rm com}$ falls to zero at the resonance values $m,n=1,1$ and $1,2$, as forecast, but has sharp peaks just below the resonances that arise from the comparatively large values of $(\det L)^{-1}$ (figure 3). Figure 4(b) shows the neighbourhood of the resonance value $\kappa a=3.83$ on a larger scale. As N increases, the peaks in $j^{\rm com}$ get higher and narrower and move to the right (figure 4(c)), with the curve always reaching zero at the resonance values. Eventually all this behaviour crowds into a series of singularities at the resonance values.

The difference between $j^{\rm com}$ and $j^{\rm true}$ defines a residual current $j^{\rm res}$. The curve for $|j^{\rm res}|$ at $N=40$ shows how it is large near the resonances but relatively small in between them. In the limit $N\to\infty$ $|j^{\rm res}|$ becomes uniformly zero except for a series of discrete spikes at the resonance values.

The source of the computational problems is now clear. Considering only a single Fourier component, the discretized integral equation is computing an approximation not to the smooth $j^{\rm true}$ curve, but to the same curve decorated with infinitely narrow spikes at the resonances. At the same time the computed values at the resonances themselves are tied down to zero. For finite N the result is broadened peaks just below the resonances (why they are below rather than above is not apparent).

Still considering only the mth Fourier component of the incident plane wave, suppose κa is fixed at a value not corresponding to any of the zeros of $J_m(\kappa a)$. As N is increased the computed current density $j_z^{\rm com}$ will eventually approach the correct one $j_z^{\rm true}$, because the bad peak will ultimately lie to the right of the selected κa, but this could require an impractically large N. Thus, for most values of κa the discretized model computes a current density that immediately begins to approach the correct one as the size of the matrix is increased. But

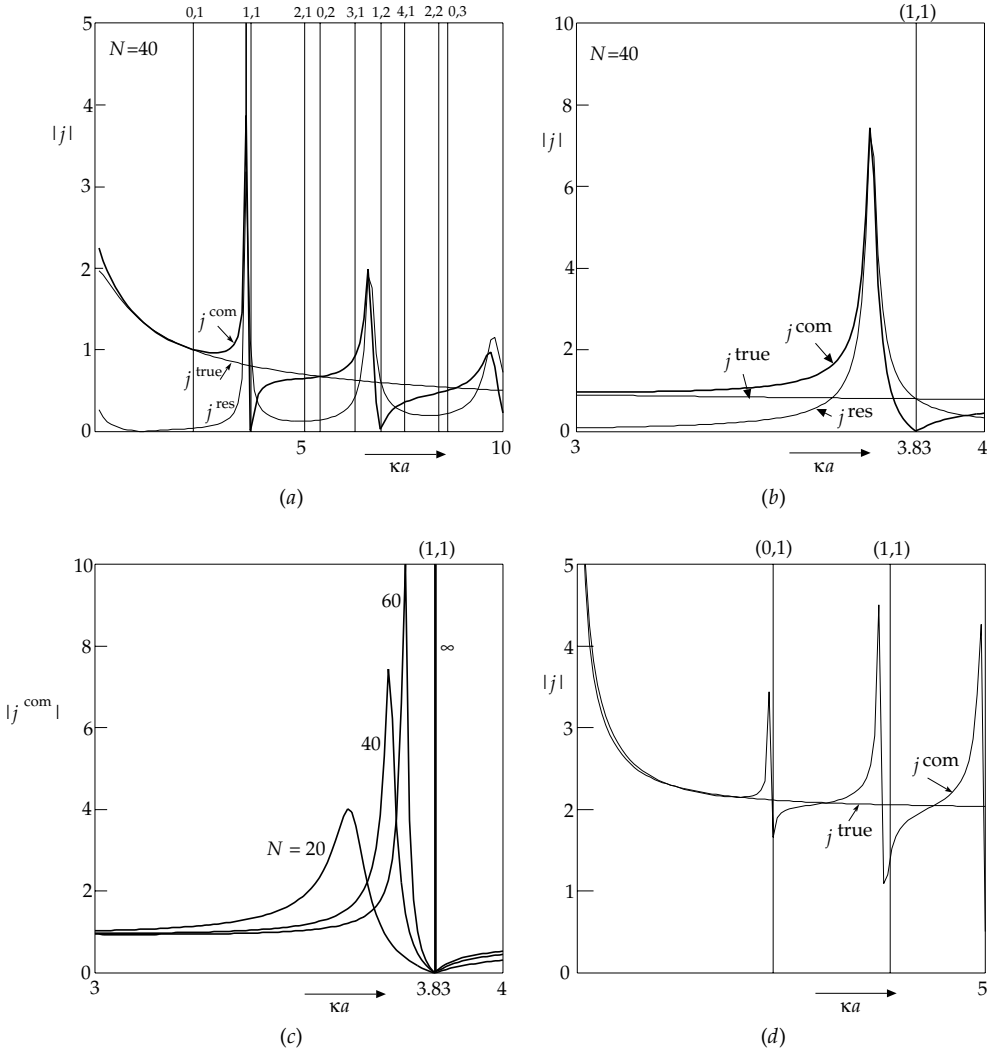

Figure 4. E-polarization. For (*a*), (*b*) and (*c*) only the $m = 1$ Fourier component of the plane incident wave is present; for (*d*) the complete plane wave is present. (*a*) The magnitudes of the resulting $m = 1$ components of the various j are plotted against κa for $N = 40$. The resonance values of κa are indicated. (*b*) The neighbourhood of the (1,1) resonance on a larger scale. (*c*) The approach of the $|j^{\mathrm{com}}|$ curve to the limit as $N \to \infty$. (*d*) $|j_z^{\mathrm{com}}|$ and $|j_z^{\mathrm{true}}|$ at $\theta = 0$, using $N = 40$.

if κa happens to lie between one of the bad peaks and the resonance value, the error will increase to a large value, as N increases and the peak passes through from left to right, before it eventually decreases to zero. However large the matrix, the bad bands between the peaks and the resonances will always exist.

When the complete plane wave is incident $j_z^{\mathrm{com}}(\theta)$ contains a mixture of Fourier components, one from the tail of each resonance, unless κa is near to a peak of $j_z^{\mathrm{com}}(\theta)$ for a particular m, in which case that Fourier component dominates. To illustrate this, figure 4(*d*) plots $\left|j_z^{\mathrm{com}}(0)\right|$ against κa, using $N = 40$, for the range $0 < \kappa a < 5$. There is anomalous behaviour near each resonance, more pronounced to its left than to its right.

3.4. Effect on the computed fields

To compute the field from the current density we use the discretized version of equation (7) for E_z^{sc} and add E_z^{inc}. $j_z^{true}(\theta)$ then generates an external field that agrees with equation (3) to an accuracy (using $N = 20$) of typically 1 part in 10^6 or better. It also generates an internal field that cancels the incident field, as it should. On the other hand, when $j_z^{com}(N, \theta)$ is inserted in the discretized version of equation (7) its most conspicuous effect is to produce a false non-zero total field inside the boundary. Figure 5 shows an example, choosing κa =6.3799, which is one of the $m = 3$ resonances. The complete incident plane wave is present and in figure 5(b) the $\cos 3\theta$ symmetry of the internal field is evident—but it is only approximate. The explanation is as follows.

With a general κa, consider first the effect of the mth Fourier (Bessel) component of the incident plane wave of equation (1). It produces a computed current density $j_z^{com}(\theta)$ that is proportional to $\cos m\theta$. But we know that the true current density $j_z^{true}(\theta)$, which is also proportional to $\cos m\theta$, generates an internal scattered standing wave proportional to $J_m(\kappa r)\cos m\theta$ that just cancels the mth component of the incident field. Unless κa is such that $J_m(\kappa a) = 0$, this standing wave will not be a normal mode of the circle, because $r = a$ is not a nodal line. In just the same way the computed current density $j_z^{com}(\theta)$ also generates an interior standing wave, not a normal mode, proportional to $J_m(\kappa r)\cos m\theta$, but because $j_z^{com}(\theta) \neq j_z^{true}(\theta)$ for finite N it cannot exactly cancel the incident field. Thus, adding the scattered and incident fields, we are left with an unwanted interior field that is a standing wave proportional to $J_m(\kappa r)\cos m\theta$. If $J_m(\kappa a) = 0$, $j_z^{com}(\theta) = 0$ and the standing wave is just the completely uncancelled mth component of the incident field, namely $\varepsilon_m(-\mathrm{i})^m J_m(\kappa r)\cos m\theta$. The effect will be most pronounced when κa is at a peak of the $j_z^{res}(\theta)$ curve for a given m and N.

For the complete incident plane wave the unwanted interior field will be a superposition of the standing waves coming from each Fourier component, and so it will not itself be a pure standing wave. This is illustrated in the phase patterns on the right of figures 5(b) and (c), which do not show uniform phase with jumps of π. These two figures are special because κa is at a resonance. In contrast, figures 6(a) and (b) are for $\kappa a = 1$, which is quite far from a resonance. The error in $j_z^{com}(\theta)$ is quite small and so the computed interior field is zero within the accuracy of the plot.

Coming now to the exterior field, it has the correct form (compare figures 5(a) and (b)). Table 1 compares the errors in the external field at particular points for $N = 20$ and $N = 40$, and shows that, in general, doubling N halves the error. With $N = 20$ and excluding κa near resonance, the errors are of the order of 9–16%, which improves to 5–8% with $N = 40$. One per cent accuracy would require $N \approx 200$.

On the other hand, when κa is just below a resonance there can be a large error in the external field (penultimate line of table 1), because of the error in $j_z^{com}(\theta)$. In principle, if κa and N were increased together in suitable combination, the error would increase without limit.

4. B-polarization

The analysis for B-polarization follows similar lines. Although the derivation of the integral equation is a little more complicated, the final results are much the same.

Let the scalar u now stand for B_z. The boundary condition on the cylinder is then $\partial u/\partial r \propto E_\theta = 0$ instead of $u = 0$, and the current density, which is now in the θ direction, is given by the discontinuity in u. Specifically, let the incident wave be the same as before, with unit amplitude of the electric vector, but with **B** directed along O_z, so that

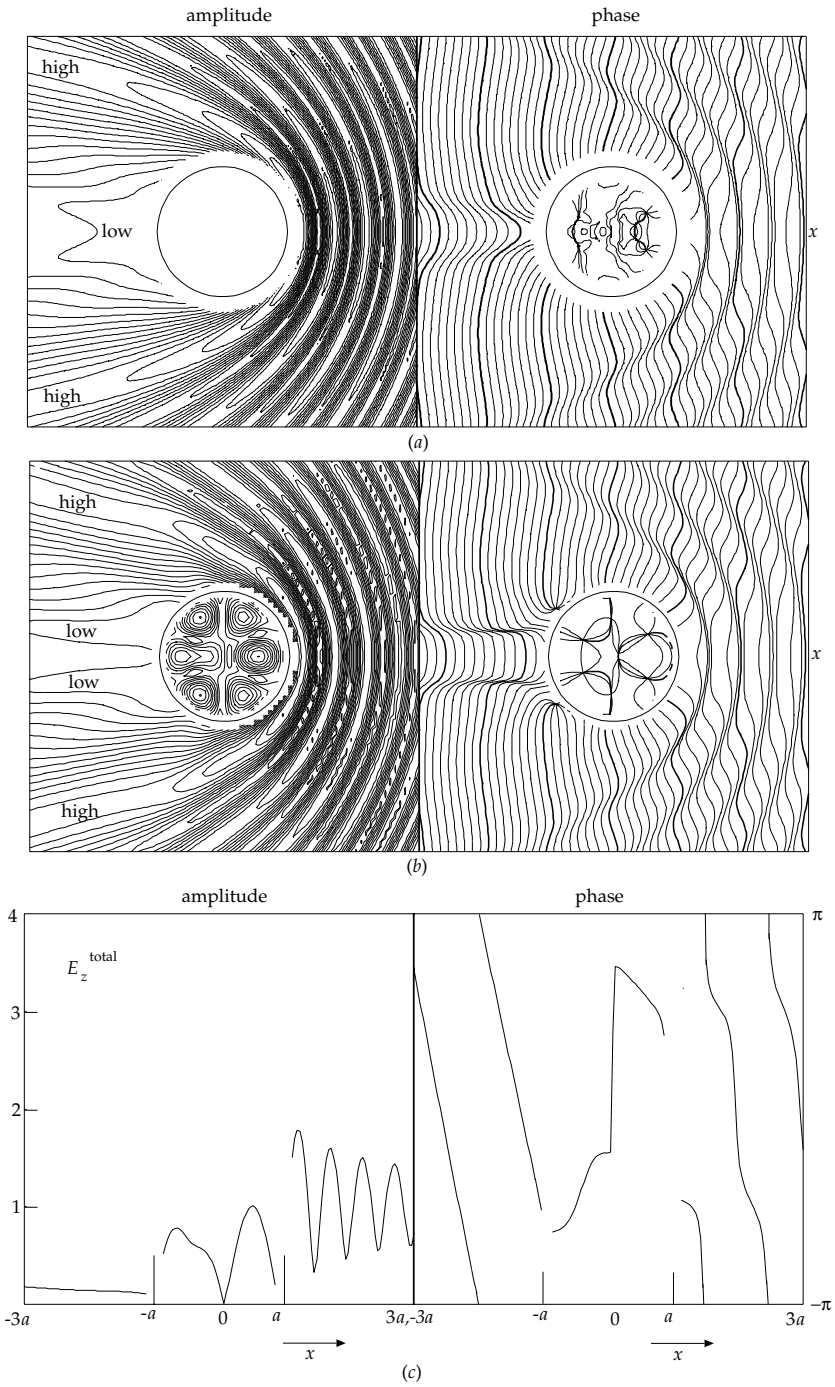

Figure 5. E-polarization. $\kappa a = \beta_{31} = 6.3799$. Contour maps of the amplitude (left) and phase (right) of E_z^{total}, computed using (*a*) the exact equation (3) and (*b*) $j_z^{\text{com}}(\theta)$ for $N = 80$. The contour interval for amplitude is 0.1 and for phase $\frac{1}{4}\pi$. (*c*) *x*-cut of the field in (*b*). For $|x| > a$ the exact curves from equation (3) are almost the same. The blank annulus near the boundary contains points nearer the boundary than the spacing of the sample points on the circle.

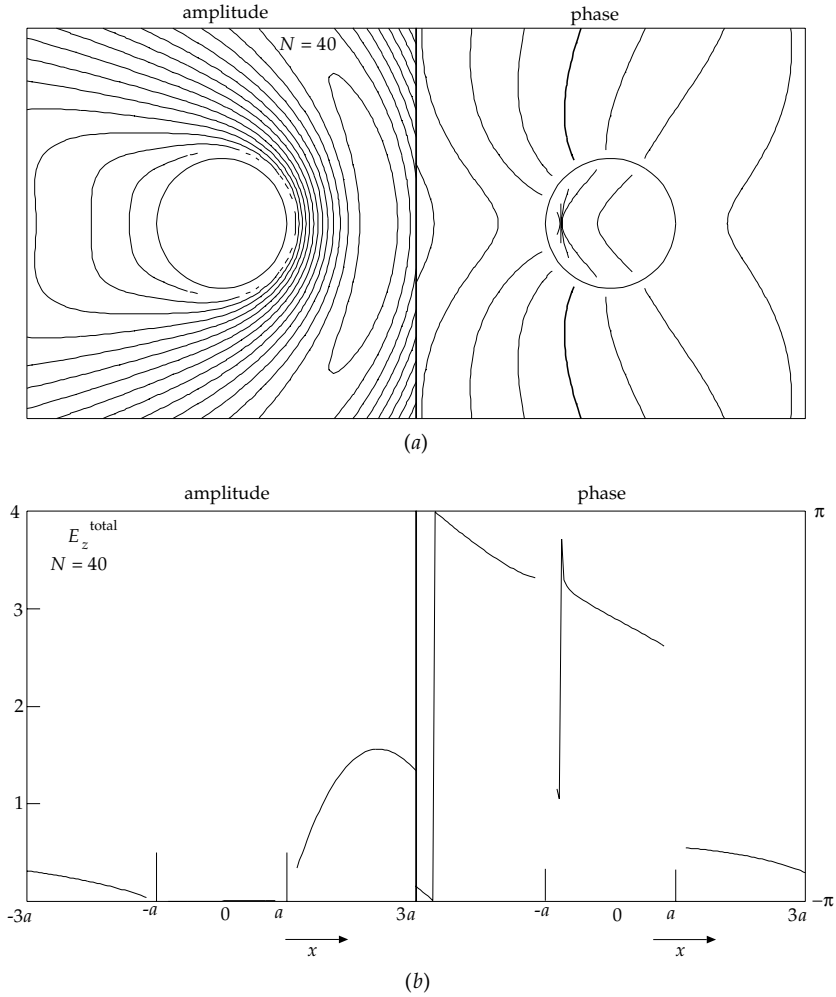

Figure 6. E-polarization. As figure 5 but for $\kappa a = 1$.

Table 1. Error in the external field (E-polarization).

	Error(%)			
	$N = 20$	$N = 20$	$N = 40$	$N = 40$
	$x = 2a$	$x = -2a$	$x = 2a$	$x = -2a$
κa	$y = 0$	$y = 0$	$y = 0$	$y = 0$
0.1	13	16	6.2	8.0
0.5	3	7	2.0	3.3
1	0.7	1.3	0.3	0.7
2	5	7	2.4	3.4
3	40	9	19.8	5.4
3.627[a]	58	410	20.3	47.8
3.83[b]	16	85	8.0	40.0

[a] Peak of j_z^{res} for $m = 1, N = 20$.
[b] $\kappa a = \beta_{11}$.

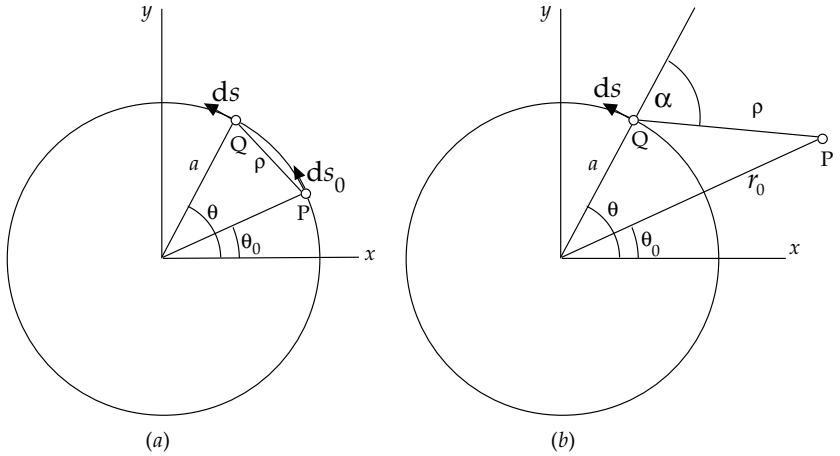

Figure 7. B-polarization. Notation.

$u^{\text{inc}} = B_z^{\text{inc}} = (1/c)\,\mathrm{e}^{-\mathrm{i}\kappa x}$. Expanding this incident wave as equation (1) and the scattered wave as equation (2), the analogue of equation (3), for $r \geqslant a$, is found as

$$u^{\text{total}} = c^{-1}\sum_{m=0}^{\infty}\varepsilon_m(-\mathrm{i})^m\cos m\theta\left[J_m(\kappa r) - \frac{J'_m(\kappa a)}{H'_m(\kappa a)}H_m(\kappa r)\right]$$
$$= c^{-1}\sum_{m=0}^{\infty}\varepsilon_m(-\mathrm{i})^m\cos m\theta\left[J_m(\kappa r) - \frac{(m/\kappa a)J_m(\kappa a) - J_{m+1}(\kappa a)}{(m/\kappa a)H_m(\kappa a) - H_{m+1}(\kappa a)}H_m(\kappa r)\right]. \tag{13}$$

Assuming that $B_z^{\text{total}} = 0$ inside the circle $r = a$, $\mu_0 j_\theta(\theta) = -B_z^{\text{total}} = -u^{\text{total}}$ just outside. On using the Wronskian relation it then follows that

$$j_\theta(\theta) = (2/\pi)Z_0^{-1}\sum_{m=0}^{\infty}\varepsilon_m(-\mathrm{i})^{m+1}\frac{\cos m\theta}{mH_m(\kappa a) - \kappa a H_{m+1}(\kappa a)}. \tag{14}$$

This exact $j_\theta(\theta)$ will be designated as $j_\theta^{\text{true}}(\theta)$.

4.1. Solution in terms of the current sources

The analogue of equation (8) is obtained as follows. Consider vector line elements $\mathrm{d}\mathbf{s}_0$, $\mathrm{d}\mathbf{s}$ on the circle at P and Q respectively (figure 7(*a*)), with lengths $\mathrm{d}s_0 = a\,\mathrm{d}\theta_0$, $\mathrm{d}s = a\,\mathrm{d}\theta$. Unlike the case of E-polarization there is now a non-zero electric charge density $q(s)$ on the circle given by $\partial j_\theta/\partial s = \mathrm{i}\omega q(s)$. $\mathbf{E}^{\text{sc}}$ at P, due to the current density, is given in terms of the electrostatic potential ϕ_0 and the magnetic potential $\mathbf{A}_0$ as $\mathbf{E}^{\text{sc}} = i\omega\mathbf{A}_0 - \nabla\phi_0$.

At P

$$\phi_0 = \frac{\mathrm{i}a}{4\varepsilon_0}\int \mathrm{d}\theta\, q(\theta)H_0(\kappa\rho), \qquad \text{where} \quad \rho = \left|2a\sin\frac{1}{2}(\theta - \theta_0)\right|,$$

with gradient

$$\nabla\phi_0 = \frac{\mathrm{i}}{4\varepsilon_0}\int \mathrm{d}\theta\, q(\theta)\frac{\partial H_0(\kappa\rho)}{\partial\theta_0}.$$

Also at P

$$\mathbf{A}_0 = \frac{\mathrm{i}\mu_0}{4}\int \mathrm{d}\mathbf{s}\; j_\theta(\theta)H_0(\kappa\rho).$$

Therefore, the tangential component of $\mathbf{E}^{\mathrm{sc}}$ is

$$\begin{aligned} E_\theta^{\mathrm{sc}} &= \mathrm{i}\omega A_\theta - \partial\phi_0/\partial s_0 \\ &= -\frac{\omega\mu_0 a}{4}\int \mathrm{d}\theta\cos(\theta-\theta_0)\,j_\theta(\theta)H_0(\kappa\rho) - \frac{\mathrm{i}}{4\varepsilon_0}\int \mathrm{d}\theta\; q(\theta)\frac{\partial H_0(\kappa\rho)}{\partial\theta_0}. \end{aligned}$$

In the second term substitute $q = (1/\mathrm{i}\omega)\partial j_\theta/\partial s = (1/\mathrm{i}\omega a)\partial j_\theta/\partial\theta$, and then integrate by parts to give $+\frac{1}{4\varepsilon_0\omega a}\int \mathrm{d}\theta\; j_\theta(\theta)\frac{\partial^2 H_0(\kappa\rho)}{\partial\theta_0\partial\theta}$. Hence, since $\partial\rho/\partial\theta = -\partial\rho/\partial\theta_0$,

$$E_\theta^{\mathrm{sc}} = -\frac{Z_0 a}{4}\int \mathrm{d}\theta\, j_\theta(\theta)\left[\kappa H_0(\kappa\rho)\cos(\theta-\theta_0) + \frac{1}{\kappa a^2}\frac{\partial^2 H_0(\kappa\rho)}{\partial\theta^2}\right]. \tag{15}$$

The boundary condition is $E_\theta^{\mathrm{sc}} = -E_\theta^{\mathrm{inc}}$ and $E_\theta^{\mathrm{inc}} = -\cos\theta_0\,\mathrm{e}^{-\mathrm{i}\kappa a\cos\theta_0}$ at the point (a, θ_0). Therefore, the analogue of the boundary integral equation (8) is

$$-\frac{Z_0 a}{4}\int \mathrm{d}\theta\; j_\theta(\theta)\left[\kappa H_0(\kappa\rho)\cos(\theta-\theta_0) + \frac{1}{\kappa a^2}\frac{\partial^2 H_0(\kappa\rho)}{\partial\theta^2}\right] = \cos\theta_0\,\mathrm{e}^{-\mathrm{i}\kappa a\cos\theta_0}. \tag{16}$$

4.2. Computing the field

The scattered field $\mathbf{B}$ is obtained from $\mathbf{A}$ by using the equation $\mathbf{B} = \mathrm{curl}\mathbf{A}$. Thus at the point $P = (x, y)$, $B_z^{\mathrm{sc}} = \partial A_y/\partial x - \partial A_x/\partial y$ and

$$A_x = \frac{\mathrm{i}\mu_0 a}{4}\int \mathrm{d}\theta\; j_x(\theta)H_0(\kappa\rho) \qquad A_y = \frac{\mathrm{i}\mu_0 a}{4}\int \mathrm{d}\theta\; j_y(\theta)H_0(\kappa\rho)$$

where $j_x = -j_\theta\sin\theta$, $j_y = j_\theta\cos\theta$ and $\rho = \sqrt{(x-a\cos\theta)^2 + (y-a\sin\theta)^2}$.
Carrying out the differentiations, using $H_0' = -H_1$, we find

$$\begin{aligned} B_z^{\mathrm{sc}} &= -\frac{\mathrm{i}\mu_0\kappa a}{4}\int \mathrm{d}\theta\; j_\theta(\theta)H_1(\kappa\rho)\frac{x\cos\theta + y\sin\theta - a}{\rho} \\ &= -\frac{\mathrm{i}\mu_0\kappa a}{4}\int \mathrm{d}\theta\; j_\theta(\theta)H_1(\kappa\rho)\cos\alpha \end{aligned} \tag{17}$$

where α is the angle shown in figure 7(b).

4.3. Numerical results

Figures 8(a) and (b) show distributions of $j_\theta^{\mathrm{true}}(\theta)$ found from equation (14) for a number of values of κa. Oscillations with a period of $\frac{1}{2}\lambda$ occur towards the rear. These current densities substituted into equation (17) produce no field inside the circle.

The integral equation (16), to be expressed in discrete form, is very similar to equation (8) except for the presence of the second derivative H_0''. On the face of it this has a θ^{-2} singularity. In the discretization we approximate H_0'' by using the second differences of the H_0 values. Then a matrix equation of the form (11) is obtained. Where infinite values of H_0 occur in the matrix L_{ik} they are replaced by finite values exactly as described in section 3.2 and the matrix equation is solved for the j values. The justification for treating the singularity in this way is as follows. Integrating twice by parts and making use of the periodic nature of the solution, converts the integrand $j_\theta H_0''$ to $j_\theta'' H_0$, so that the only singularity is in H_0 and is logarithmic. One could then go on to solve the matrix equation for the known linear

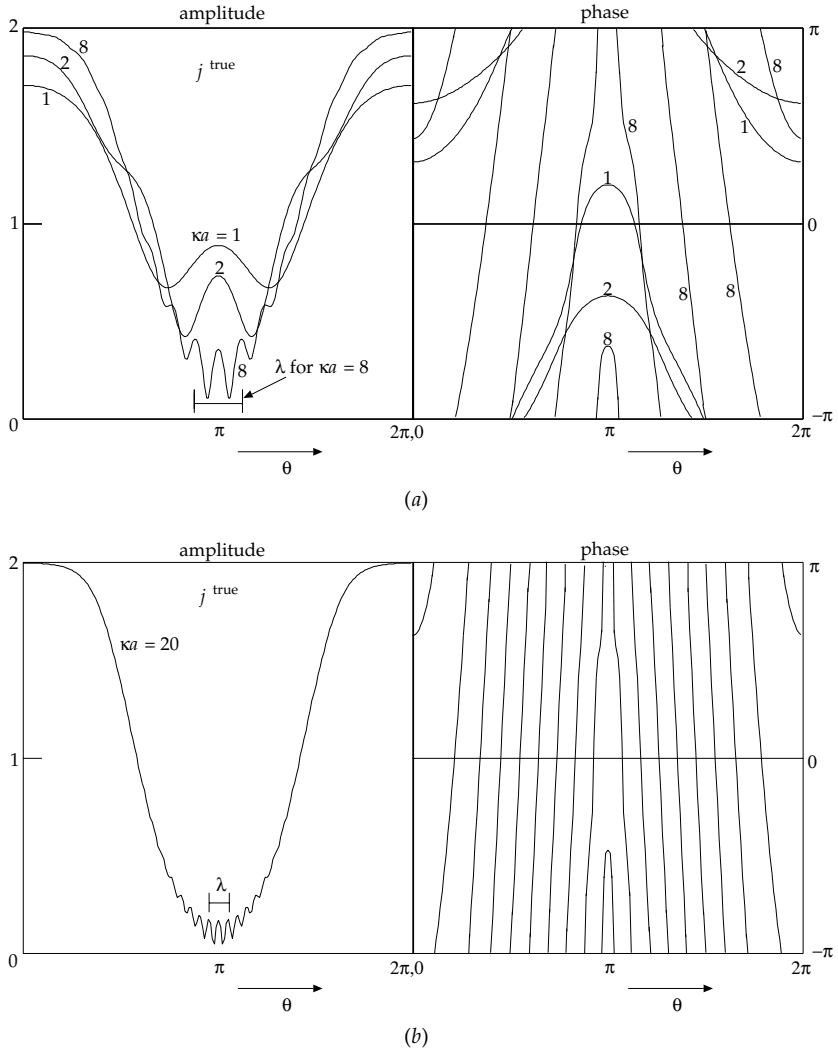

Figure 8. B-polarization. $j_\theta^{\text{true}}(\theta)$ for different values of κa.

combination of j and j'' and then integrate to find j itself. However, it is computationally equivalent, and much simpler, to do what was described above.

Just as with E-polarization the solutions for the current density j_θ^{com} include a residual part $j_\theta^{\text{res}}(\theta)$ that produces a spurious internal field, and has some effect on the external field. A plot of $\det(L_{ik})$ against κa is similar to that in figure 3, but trends the opposite way, downwards, and shows dips just to the left of the zeros of $J'_m(\kappa a)$.

As for E-polarization $j_\theta^{\text{res}}(\theta)$ is defined as $j_\theta^{\text{com}}(\theta) - j_\theta^{\text{true}}(\theta)$. Suppose we consider only the mth Fourier component of the whole field, and suppose that κa is chosen to correspond to an mth order resonance; thus $J'_m(\kappa a) = 0$. With E-polarization we were able to expand R_i on the right-hand side of equation (11) as a Fourier cosine series by inspection of equation (1), but with B-polarization the factor $\cos\theta_0$ on the right-hand side of equation (16) prevents this. The remedy is to rederive R_i, by using the general expression, $E_\theta = (c/\mathrm{i}\kappa)(\partial B_z/\partial r)$ and the

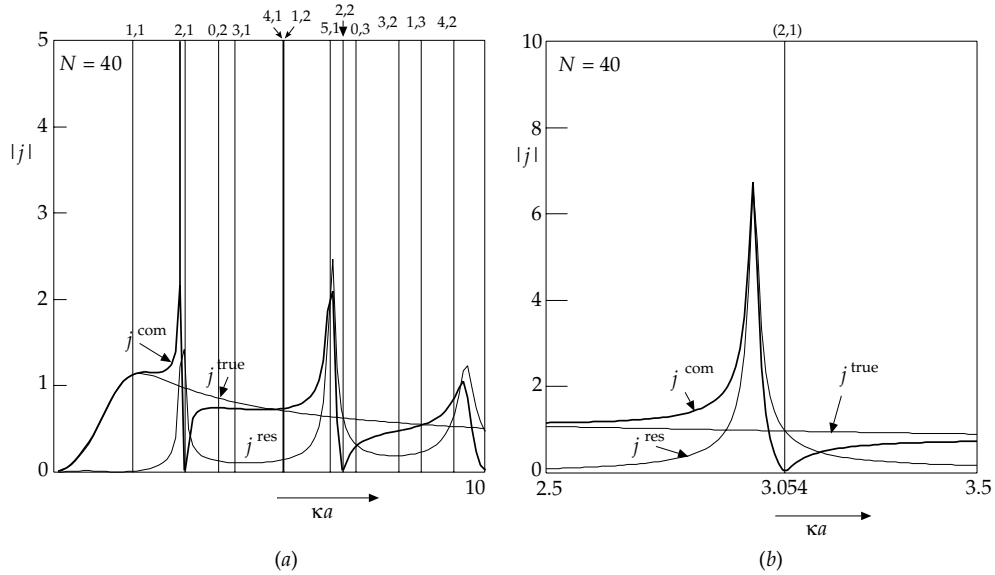

Figure 9. B-polarization. The analogue of figure 4. Only the $m = 2$ Fourier component of the plane incident wave is present. The resulting $m = 2$ components of the various j are plotted against κa. (*a*) The resonance values of κa are indicated, the (2, 1) and (2, 2) resonances being picked out. For $\kappa a < 1$ the j^{true} and j^{com} curves are nearly coincident. (*b*) The neighbourhood of the (2, 1) resonance on a larger scale.

expansion (1). Thus,

$$B_z^{\text{inc}} = c^{-1}\,\mathrm{e}^{-\mathrm{i}\kappa x} = c^{-1}\sum_{m=0}^{\infty}\varepsilon_m(-\mathrm{i})^m J_m(\kappa r)\cos m\theta$$

and, at (a, θ_0),

$$-E_\theta^{\text{inc}} = -\sum_{m=0}^{\infty}\varepsilon_m(-\mathrm{i})^{m+1} J_m'(\kappa a)\cos m\theta_0$$

which is in the required form of a cosine series. With $\theta_0 = \theta_i$ the mth term on the right-hand side is the necessary expression for R_i. But we have specified that $J_m'(\kappa a) = 0$. Hence, in the matrix equation $j_\theta^{\text{com}} = L^{-1}R$, considering only the mth component, R is now zero, and L^{-1} is not infinite. Thus $j_\theta^{\text{com}} = 0$. Just as for E-polarization, if $j_\theta^{\text{com}}(N, \theta)$ is zero it can generate no scattered field; the cylinder is transparent.

Figures 9(*a*) and (*b*) for B-polarization are analogous to figures 4(*a*) and (*b*) for E-polarization. For a particular value of m ($m = 2$) they show the amplitude of the mth Fourier component of j_θ^{com}, j_θ^{true} and j_θ^{res} as the radius κa is varied. When κa coincides with one of the zeros of $J_m'(\kappa a)$, j_θ^{com} becomes zero and $j_\theta^{\text{res}} = -j_\theta^{\text{true}}$. The internal field, which should not be present at all, is then simply the mth component of the incident field.

Figure 10 is an example of a field of B_z^{total} at a value of κa for the resonance $m = 3$, $n = 1$, computed from equation (17) after adding the incident field. The approximate three-fold symmetry ($\cos 3\theta$) of the internal field is clearly seen, even though other Fourier components with $m = 1, 2, 4$ and 5 are present in the current density. The whole picture is thus quite similar to that for E-polarization.

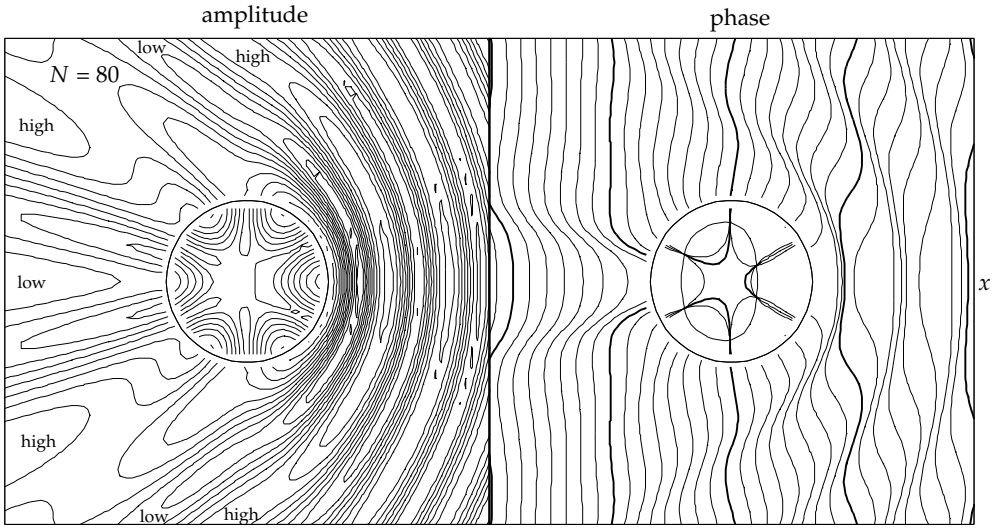

Figure 10. B-polarization. The field of B_z^{total} for $\kappa a = 4.2012$, corresponding to the resonance (3, 1).

5. Summary

For both E- and B-polarizations the wave scattered from the cylinder may be regarded as produced by a current density in the cylindrical boundary $j^{\text{true}}(\theta)$, where θ is the polar angle, and this can be readily computed from standard theory. Alternatively, the boundary may be divided into N intervals and the current density, now denoted $j^{\text{com}}(\theta)$, may be computed by expressing the appropriate integral equation in discretized form. The difference between $j^{\text{com}}(\theta)$ and $j^{\text{true}}(\theta)$ defines a residual current density $j^{\text{res}}(\theta)$ that is purely an artefact of the discretization. It arises because the discretized integral equation is computing an approximation not to the smooth $j^{\text{true}}(\theta)$ curve, but to the same curve decorated with infinitely narrow spikes at the resonances. Provided the radius is not chosen to correspond to an internal resonance, $j^{\text{res}}(\theta)$ does approach zero as N increases, but in an unusual way: if the radius is just below a resonance value, $j^{\text{res}}(\theta)$ can increase to large values before it decreases. The consequence is a correspondingly large error in the scattered field, but, most notably, the appearance of an internal field when none at all should be present; this consists of a mixture of standing waves, not normal modes of the cylinder (except at resonance), one from each Fourier component of the incident plane wave.

Acknowledgments

I am grateful to a referee for very helpful comments, to Professor M V Berry for pointing out the connection with the inside–outside duality encountered in planar billiards and to Professor U Smilansky for a discussion.

References

Benthien W and Schenck A 1997 Nonexistence and nonuniqueness problems associated with integral equation methods in acoustics *Comput. Struct.* **65** 295–305

Berry M V 1994 Evanescent and real waves in quantum billiards and Gaussian beams *J. Phys. A: Math. Gen.* **27** L391–8

Born M and Wolf E 1999 *Principles of Optics* 7th edn (Cambridge: Cambridge University Press)

Burton A J and Millet G F 1971 The application of integral equation methods to the numerical solution of some exterior boundary-value problems *Proc. R. Soc. Lond.* A **323** 201–10

Chen I L, Chen J T, Kuo S R and Liang M T 2001 A new method of true and spurious eigensolutions of arbitrary cavities using the continuous Helmholtz exterior integral equation formulation method *J. Acoust. Soc. Am.* **109** 982–98

Dietz B, Eckmann J-P, Pillet C-A, Smilansky U and Ussishkin I 1995 Inside-outside duality for planar billiards: a numerical study *Phys. Rev.* E **51** 4222–31

Kleinman R E and Roach G F 1974 Boundary integral equations for the three-dimensional Helmholtz equation *SIAM Rev.* **16** 214–36

Luz M G E da, Lupo-Sax A S and Heller E J 1997 Quantum scattering from arbitrary boundaries *Phys. Rev.* E **56** 2496–507

Martin P A 1982 Acoustic scattering and radiation problems, and the null-field method *Wave Motion* **4** 391–408

Morse P M and Feshbach H 1953 *Methods of Theoretical Physics* Part II (New York: McGraw-Hill)

Nye J F 2002 Numerical solution for diffraction of an electromagnetic wave by slits in a perfectly conducting screen *Proc. R. Soc. Lond.* A **458** 401–27